ES
Engineering and Science

Estudo Numérico Via Elementos Finitos do Comportamento Estrutural do Pavimento Rígido de Aeródromos

Numerical Study Via Finite Element Analysis of the Structural Behavior of Rigid Pavement of Aerodromes

[1]Eduardo Matiola Souza, [2]Rodrigo Alves e Silva, [3]Albert Willian Faria

[1]Engenheiro Civil – Universidade Federal do Triângulo Mineiro (matiola.eduardo@gmail.com)
[2]Candidato a PhD – GeoEngineering Centre at Queens-RMC, Queen's University, Kingston, ON, Canada (r.esilva@queensu.ca)
[3]Professor Associado do Departamento de Engenharia Civil – Universidade Federal do Triângulo Mineiro (albert.faria@uftm.edu.br)

Resumo: Esse artigo desenvolve um modelo numérico 3D, via Método dos Elementos Finitos - MEF, do pavimento de concreto de um aeródromo em contato com as rodas duplas de uma aeronave. O pavimento consiste em seis placas de concreto ligadas por meio de barras de transferência e juntas longitudinais assentadas em um solo de apoio de rigidez *k*. Através dos resultados numéricos via MEF obtidos, pôde-se validar numericamente o modelo numérico desenvolvido através de resultados disponível na literatura científica, analisando a influência das barras de transferência, juntas longitudinais e rigidez do solo sobre a distribuição das deflexões do pavimento submetido ao carregamento dinâmico. Pode-se constatar que as barras de transferência reduziram em torno de 77% as deflexões. Além disso, é apresentada uma metodologia para o dimensionamento da espessura do pavimento e da resistência característica do concreto baseada no critério de falha de Mohr-Coulomb, obtendo-se uma resistência característica mínima do concreto de 28 MPa para uma espessura de 0.305m.

Palavras-chave: Pavimento de concreto de um aeródromo. Análise 3D via elementos finitos. Barras de transferência. Juntas transversais.

ABSTRACT: The present study develops a 3D numerical model of the concrete pavement system of aerodromes in contact with the main landing gear of aircrafts using Finite Element Method (FEM). The pavement system used in the analysis consisted of six concrete slabs overlaying a subgrade medium with stiffness *k*. Doweled bars are considered for the pavement transverse joints while aggregate interlocks are considered for longitudinal joints. A parametric study was conducted to validate the model numerically, as well as to investigate the influence of the doweled bars, aggregate interlocks and subgrade stiffness on the pavement deflections when it is subjected to a dynamic load. About 77% decrease in deflection was attained due to the presence of doweled bars. This study additionally presents a methodology for designing the pavement thickness and the compressive strength of concrete based upon the Mohr-Coulomb's failure criterion. It is found that for a pavement thickness of 0.305m the minimum compressive strength of concrete should be 28 MPa.

Keywords: Concrete airfield pavement. Three-dimensional finite element analysis. Dowel bars. Transverse joint.

1. INTRODUCTION

Rigid pavements of aerodromes are subjected to loads of considerably higher magnitudes compared to those from highway networks or bus corridors, although involving less repetitive cycles. Naturally, cracks may develop over time due to variations of temperature and rainfall, which poses an issue deserving special attention. An interesting alternative to the analytical methods comprising abacuses and empirical formulations on the prediction of cracks and, thus, degradation of the rigid pavement in aerodromes, is the use of Finite Element Method (FEM) assessing the pavement stress-state and mechanical behavior (BALBO, 2009).

Practices for the design of rigid pavements in aerodromes traditionally follow either the *Portland Cement Association* (PCA), *American Concrete Pavement Association* (ACPA),

E&S - Engineering and Science ISSN: 2358-5390 DOI: 10.18607/ES202099827 Volume 1, Edição 9

Federal Aviation Administration (FAA) or the *Layered Elastic Design Federal Aviation Administration* (LEDFAA) (BALBO, 2009; DELATTE, 2008). The PCA, ACPA and LEDFAA methods employ the concepts from the Elasticity Theory rather than the traditional Westergaard Theory employed by the FAA. The FAA method, however, is not sensible to the stiffness *k* of the underlying subgrade medium, that is to say, *k* has no effect on the design of the pavement thickness (DELATTE, 2008). Several FEM software are built based on the guidelines from the aforementioned associations, e.g. the FAARFIELD and ACPA AirPave software based on the procedures from LEDFAA and PCA, respectively (DELATTE, 2008). Kim *et al.* (2014) employed the FAARFIELD software to analyze the distribution of stresses on the concrete pavement due to temperature-induced loads from different aircrafts. They found that the results were in good agreement with stresses observed in the field.

Few studies addressing the structural behavior of connecting joints in concrete pavements are available in the scientific literature, for instance, Kim & Hjelmstad (2003) and Yan-cong & Ling-ling (2016). The former evaluated various aspects of the structural behavior of doweled joints in a rigid pavement modeled through 3D finite elements, particularly using the ABACUS software. The authors concluded that between 15 and 30% of the load applied by the analyzed aircraft landing gear was transferred by the doweled joints to the adjacent slabs. In the second study, the authors investigated the effect of changing the position of the doweled bars (e.g. vertical or horizontal angle, embedded depth) on its load transfer. It was verified that the horizontal angle has a negligible effect on the load transfer coefficient, but this decreases almost linearly when the vertical angle increases.

Prawesti *et al.* (2019) studied the performance of the rigid pavement of the Soekarno-Hatta International Airport, Indonesia, considering the maximum stresses and deflections over a service life of 20 years. Caliendo & Parisi (2010) developed 3D finite element models using the ABACUS software to analyze the maximum stresses at critical locations of concrete slabs, such as their interior and edges. Rodchenko (2017) modeled a concrete pavement subjected to an Airbus 380 load using the Aerodrom 380 software and concluded that the expected service life of the pavement is 70% the service life estimated using FAARFIELD. Alvappillai *et al.* (1992) developed a FEM algorithm to assess the dynamic response of a multiple, jointed rigid pavement system subjected to moving aircraft loads. Their study considered the dynamic aircraft-pavement interaction effects by modelling the aircraft landing gear as masses supported by spring-dashpot systems, and employed beam elements to model the dowel bars connecting the concrete slabs.

There is currently a paucity of national works investigating the structural behavior of rigid pavements of aerodromes using FEM, particularly under a variable subgrade stiffness (or modulus of subgrade reaction). In order to fill this gap, the present work developed a 3D FEM model to better analyze the mechanical behavior of soil-pavement systems in aerodromes when they are subjected to aircraft loads. A valuable aspect of this study hardly found in the literature is the analysis of pavement stresses and deflections in the transient domain. The commercial software ANSYS is employed, a suitable tool for numerous scientific works and well known by multinational companies of the aviation sector (such as Embraer) for the design and analysis of aircraft components.

Despite the existing investigation of connecting joints in concrete pavements, e.g. Kim & Hjelmstad (2003) and Yan-cong & Ling-ling (2016), the present study aims attention at the influence of the diameter of such joints on the deflections of concrete slabs, an aspect not so broadly discussed. In addition, the Mohr-Coulomb's failure criterion based on the Elasticity Theory for small deformations and brittle materials is employed to the analysis of principal normal stresses developed in the pavement. A minimum compressive strength of concrete (and minimum thickness) is, then, provided in face of the aircraft load studied.

2. MATERIALS AND METHODS

2.1 Pavement-subgrade system

The 3D numerical model of the rigid pavement system as well as its interaction with the adjacent subgrade medium were developed based on the study of Alvappillai *et al.* (1992): three concrete slabs arranged in the longitudinal direction and two in the transverse direction, as depicted in Figure 1. The elements providing the pavement-subgrade interaction were established with a free end in contact with the pavement, and with a fixed end in contact with the adjacent medium. The dimensions of each slab (7.620 m x 7.620 m), the system of global axes, the position of the aircraft landing gear and the direction along which it travels are also shown in the figure. A finite element algorithm was built to investigate the dynamic behavior (i.e. deflection, stresses and strains) of the concrete slabs subjected to moving aircraft loads.

Figure 1 - Schematic representation of the rigid pavement system and the aircraft landing gear

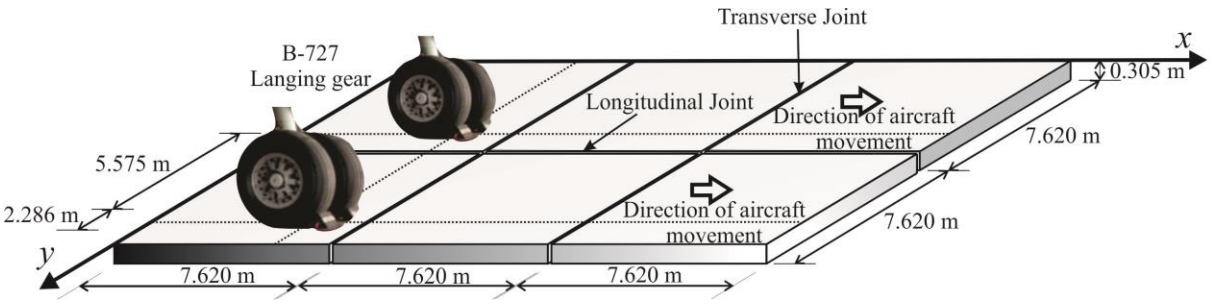

Source: Adapted from Alvappillai *et al.* (1992).

The finite element mesh adopted in the analysis is shown in Figure 2. In the figure, the notation 20@0.381 indicates that there are twenty elements 0.381 m each. Point A (x = 7.620 m and y = 7.620 m) represents the location where the dynamic response of the pavement was recorded.

Figure 2 - Finite element mesh of the concrete slabs

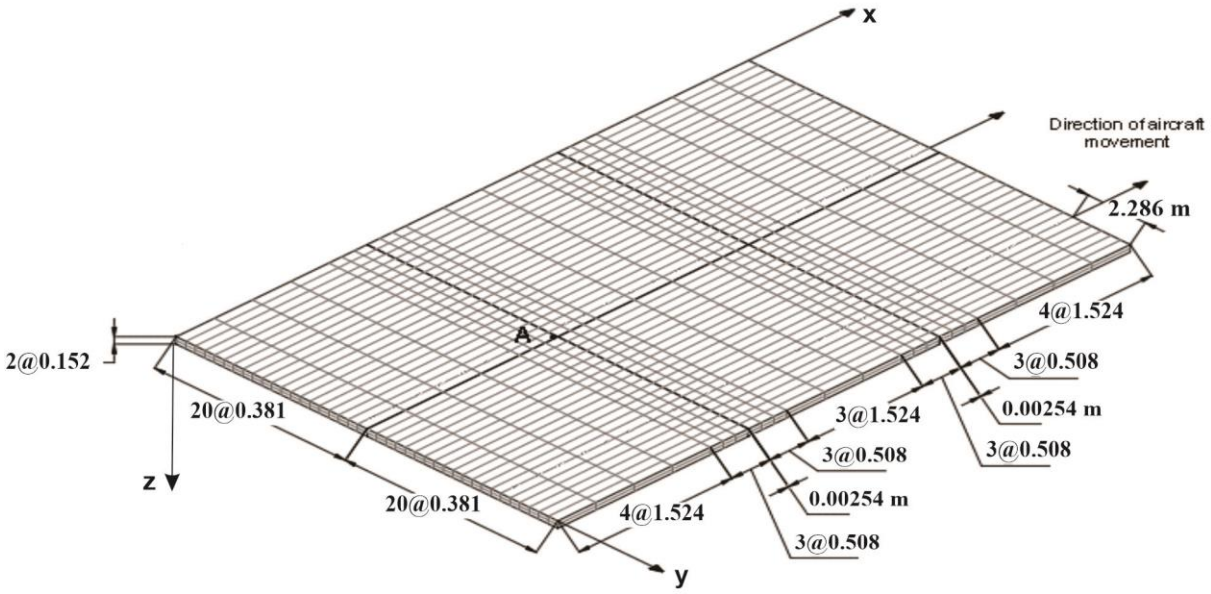

Source: Adapted from Alvappillai *et al.* (1992).

E&S - Engineering and Science ISSN: 2358-5390 DOI: 10.18607/ES202099827 Volume 1, Edição 9

The finite elements adopted consist of four-noded, rectangular thin plate elements with three degrees of freedom at each node, i.e. vertical displacement in the *z* direction and rotation about the *x* (θ_x) and *y* (θ_y) axes. The beam elements used to represent the doweled bars have only two degrees of freedom, vertical displacement in the *z* direction and rotation about the *x* (θ_x) axis. These bars are distributed along the transversal joints, as illustrated in Figure 3. It is assumed that the doweled bars are fully embedded into the pavement and that they are massless. An aggregate interlock or keyed joint is assumed for longitudinal joints, being modelled by vertical spring elements which only transfers shear forces. The pavement subgrade system is idealized by Kelvin-type viscoelastic elements represented by a number of springs and dampers connected in parallel.

Figure 3 - Finite element representation of the pavement-subgrade system and the aircraft landing gear

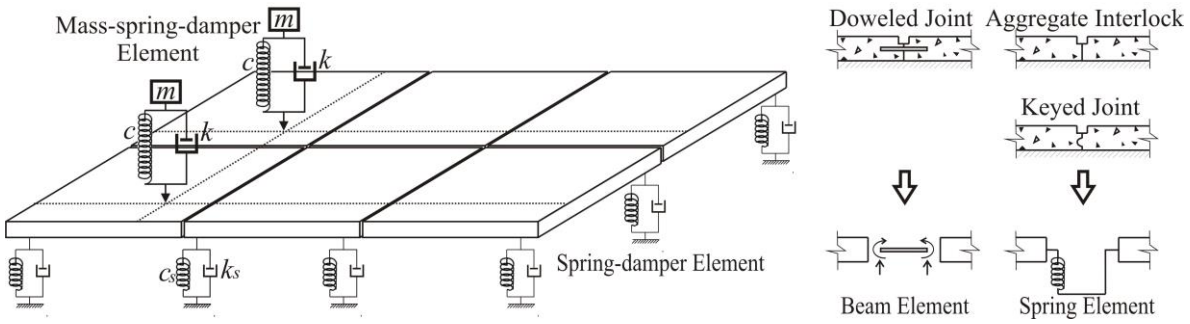

Source: Adapted from Alvappillai *et al.* (1992).

The material properties for the pavement-subgrade system adopted in this study are shown in Table 1, exhibited in both English and SI units.

Table 1 - Properties of materials used in the pavement-subgrade system

Pavement-subgrade properties:	**International System of Units**
Dimensions of concrete slabs	7.620 m x 7.620 m
Pavement thickness	0.305 m
Young's Modulus (E)	24.820 GPa
Poisson's ratio (ν)	0.150
Mass density (ρ)	2323.340 kg/m³
Modulus of subgrade reaction (k)	81434.110 kN/m³
Subgrade damping	5%
Joint properties	**International System of Units**
Transverse joints:	
Diameter of doweled bars (d)	2.540 x10^{-2} m
Spacing between doweled bars (s)	0.381 m
Joint width	2.540 x10^{-3} m
Young's modulus of doweled bars	199.950 GPa
Shear modulus of doweled bars (G)	75.840 GPa
Mass density (ρ)	7850 kg/m³
Longitudinal joints:	
Longitudinal joints are represented by very stiff vertical spring elements.	

to be continued

continuation

Table 1 - Properties of materials used in the pavement-subgrade system

Aircraft properties		
□	Spring stiffness of the aircraft suspension	17512.680 kN/m
□	Damping of the aircraft suspension	0.5%
□	Aircraft velocity	160.930 km/h

Source: Adapted from Alvappillai *et al.* (1992).

In the algorithm reproduced herein, the numerical models were developed based on two types of idealizations of moving aircraft wheel loads along the pavement (ALVAPPILLAI *et al*., 1992). In the first, *Moving Mass*, the dynamic aircraft-pavement interaction is considered by modelling the aircraft by masses supported by springs and dampers. In the second, *Moving Force*, the aircraft is assumed as a number of moving forces, neglecting the aircraft inertia.

2.2 Numerical model

This work employed the software ANSYS for the FEM modeling of the rigid pavement system, along with the elements SOLID65, BEAM188 and COMBIN40. The solid element SOLID65 was used to represent the concrete slabs of the aerodrome, while the element BEAM188 was used to represent the dowel bars at the transversal joints. The coupling element COMBIN40 was used to model the subgrade medium, the longitudinal joints and the aircraft main landing gear.

COMBIN40 has one degree of freedom at each node, either a nodal translation, rotation, pressure, or temperature, and may be used in any analysis, 2D or 3D (ANSYS, 2018). On the other hand, the element SOLID65 is used in the 3D modelling of solids with or without reinforcement bars (rebars), distributed as a reinforcement ratio. It is also applicable to reinforced composites such as fiberglass, and geological materials such as rock. Additionally, SOLID65 is capable of simulating nonlinear properties, e.g. plastic deformation, creep, crushing in compression and cracking in tension (in three orthogonal directions).

BEAM188 is a unidimensional element based on Timoshenko beam theory, wherein shear deformation effects are taken into consideration. Major advantages of BEAM188 include the elasticity and isotropic hardening plasticity models, which make it suitable for linear, large rotation/deflection, viscoelasticity, viscoplasticity, creep, initial stress import and large strain nonlinear applications (MAHMOUD, 2015; ANSYS, 2018). Mahmoud (2015) further reminds that the stiffness terms provided allow the analyzes of flexural, lateral and torsional stability problems. The association of SOLID65 and BEAM188 in the modelling of reinforced concrete has been considered in the literature (e.g. SILVA E BANDEIRA, 2019; KANDEKAR E TALIKOTI, 2019).

It is not unusual to employ the linear element LINK8 as a replacement of BEAM188 in the modelling of concrete structures. This is a uniaxial tension-compression element with three degrees of freedom at each node (translations in the nodal x, y, and z directions), with plasticity, creep, swelling, stress stiffening, and large deflection capabilities also included (ANSYS, 2018). However, as in a pin-jointed structure, no bending of the element is considered. The selection between BEAM 188 and LINK8 will depend upon the application, since each has its own special features. Compared with LINK8, BEAM188 can bear axial force, flexural moment and shearing, and can be applied to a larger range of special cases. Nevertheless, since it has a higher number of degrees of freedom, more computational effort is required.

The solid element is usually employed in the modeling of 3D solids without reinforcement bars (as in the application herein presented) and is defined by eight nodes with

three degrees of freedom each, namely, translations in the *x*, *y* and *z* directions. The beam element has two nodes with six degrees of freedom each, translations in *x*, *y* and *z*, and rotations in *x* (θ_x,), y (θ_y) and *z* (θ_z). The coupling element is a combination of a spring-slider (k_1), an ordinary spring (k_2) and a damper (c) in parallel, coupled to a gap in series. It is possible to associate a mass (m) with one or both nodal points. The element has only one degree of freedom at each node, either a nodal translation, rotation, pressure or temperature.

2.2.1 Modeling the concrete slabs using solid elements

Figure 2 illustrates the finite element mesh of the six concrete slabs, the dimensions of the elements and the system of global coordinates adopted.

From Figure 2, it can be noted that the concrete slabs were discretized with two elements throughout their thickness. In addition, 0.381 m elements were defined along the y direction, while 1.524 m and 0.508 m elements in the *x* direction. Since the coupling element COMBIN40 was used to represent three distinct components of the system (the subgrade medium, the longitudinal joints and the aircraft main landing gear) involving varying input parameters, three disparate elements were defined in this work: (1) a *spring-damper* element when consisting of a spring and a damper; (2) a *mass-spring-damper* element when consisting of a mass, a spring and a damper; and (3) a *spring* element when it is composed only by a spring.

2.2.2 Modeling the interaction of the rigid pavement-subgrade system

The coupling between the subgrade medium and the concrete slabs was modeled using spring-damper elements. ALVAPPILLAI *et al*. (1992) do not provide the arrangement of the spring-damper elements along the bottom surface of the concrete rigid plates, therefore additional considerations were made. Initially, the modulus of subgrade reaction is 81434.112 kN/m³ (see Table 1), but the spring coefficient for the COMBIN40 element must be provided in kN/m (force/length). In order to implement this change, the modulus of subgrade reaction was multiplied by the area of influence of each spring along the pavement-subgrade interface. By doing so, three sets of coupling elements were created, since the springs located on the inside of the concrete slabs have an area of influence higher than that of the springs located laterally, which, in turn, have an area of influence higher than that of the springs at the corners. For the springs located laterally, the area of influence is half the area of internal springs (0.581 m²). For the springs located at the corners, this value is one fourth the area of internal springs. Table 2 shows the value of the spring coefficient (k), i.e. the modulus of subgrade reaction, of the coupling elements according to their locations along the concrete slabs.

Table 2 - Modulus of subgrade reaction and subgrade damping according to different locations along the concrete slab

	Internal region	Lateral region	Edges
k (kN/m)	47284.228	23642.114	11821.057
ζ (%)	0.050	0.050	0.050
m (kg)	411.408	205.704	102.852
c_r (kN*s/m)	5479.717	2739.858	1369.929
c (kN*s/m)	273.898	136.949	68.475

The damping coefficient (c) of the spring-damper element was also modified, since, in the study of Alvappillai *et al.* (1992), it is provided as a percent value. By using the

expressions $c_r = 2\sqrt{k.m}$ and $\zeta = c/c_r$ from Kim *et al.* (2014), where ζ is the damping factor, *c* the damping coefficient, *k* the modulus of spring reaction representative of the subgrade medium and *m* the mass supported by the spring, *c* could be expressed in terms of [(force*time)/length]. These properties are shown in Table 2, obtained according to the locations of the spring-damper elements along the concrete slabs.

The spring-damper elements representing the subgrade medium were inserted every 1.524 m and 0.381 m the *x* and *y* directions of the concrete slabs, respectively, as depicted in Figure 4-a. The displacements in the *x*, *y* and *z* directions of all nodal points of these elements were restricted.

Figure 4 - Distribution of spring-damper elements: (a) along the entire concrete slab and (b) at the transverse joint between two slabs

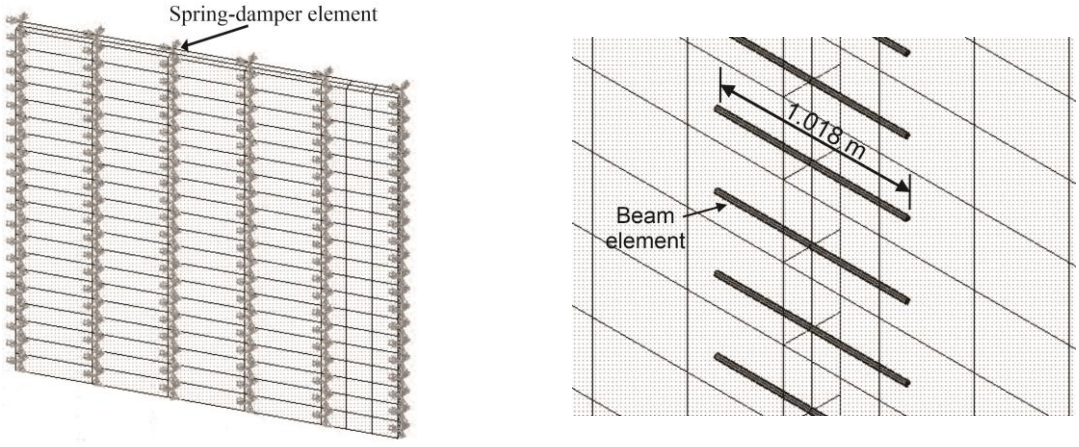

(a) (b)

2.2.3 Modeling the transversal joints using beam elements

The bars used at the transverse joints, illustrated in Figure 4-b, were positioned every 0.381 m and at the center of the concrete slab thickness, i.e. 0.1524 m from the edges in the *z* direction. The beam elements representing these steel bars were defined along the transverse joint, except for the ends, resulting in nineteen elements per slab. Differently from Alvappillai *et al.* (1992), the beam elements have a length of 1.019 m, from which 0.508 m corresponds to the length of both ends embedded into the pavement and 0.00254 m to the joint width.

2.2.4 Modeling the longitudinal joints using spring elements

The spring elements representing the longitudinal joints do not have dampers, thus only the stiffness coefficient (k_l) needs to be defined. In the work of Alvappillai *et al.* (1992), it is mentioned that the longitudinal joint is represented by very stiff vertical spring elements, but no reference value is provided. Alternatively, it was adopted herein a value corresponding to 10^6 times the modulus of spring reaction representative of the subgrade medium (see Table 2), i.e. 4.728×10^{10} kN/m. The position of spring elements was determined by connecting the nodal points of adjacent concrete slabs in the *x* direction. That resulted in six spring elements every 1.524 m for each pair of concrete slabs.

2.2.5 Modeling the aircraft main landing gear using mass-spring-damper elements

The spring constant of the mass-spring-damper element used to represent the aircraft landing gear (see Figure 3) is 17512.677 kN/m. For the damping coefficient, the same procedure described in Section 2.2.2 was done to express it in terms of [(force*time)]/length].

E&S - Engineering and Science ISSN: 2358-5390 DOI: 10.18607/ES202099827 Volume 1, Edição 9

Since each gear in the main twin assembly carries approximately 342.513 kN and the damping of aircraft suspension is 0.5%, the damping coefficient becomes 153.586 kN*s/m.

2.2.6 *Application of the aircraft dynamic load to the rigid pavement*

The aircraft considered in this study is the B-727 model with a maximum gross weight of 751.75 kN. It is assumed that the main landing gear carries 90% of the total aircraft weight (i.e. 342.513 kN on each gear) and that the remaining 10% is carried by the nose gear. Figure 5-a shows the landing gear assembly considered.

Figure 5 - Idealization of: (a) the main landing gear of the B-727 aircraft and (b) the moving load over time

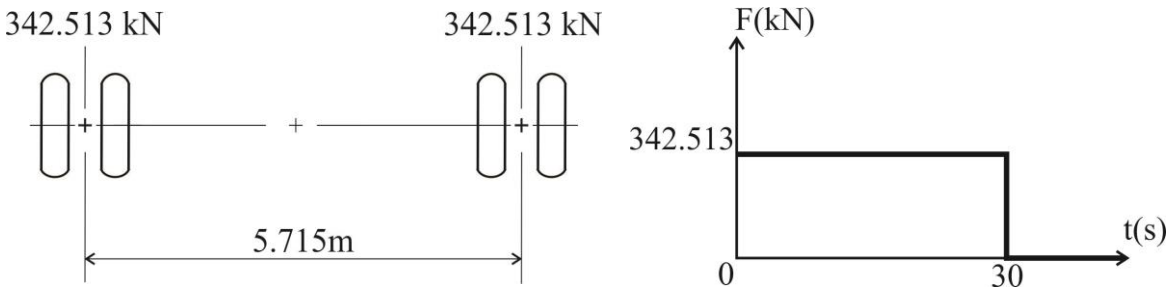

(a) (b)

For simplicity, only the main landing gear is considered in the analysis, thus neglecting the 10% from the nose gear. Additionally, a single resulting force was considered for each twin assembly of the main gear, as shown in Figure 5-a.

The load resulting from each assembly was applied following a 30-seconds interval (Figure 5-b), thus representing the aircraft at rest on the rigid pavement. This interval was chosen because, after comparing the vertical deflections at point A over different time steps, they remained constant after 30 seconds. The two vertical loads from the aircraft main landing gear (Figure 5-a) are applied at the coordinates (x_1 = 7.620 m, y_1 = 7.239 m) and (x_2 = 7.620 m, y_2 = 12.954 m), as close to point A (i.e. the point recording the dynamic response of the rigid pavement) as possible (see Figure 2).

3. RESULTS AND DISCUSSION

The validation of the numerical results obtained for the FEM pavement system implemented herein is performed based on the results of vertical deflections from Alvappillai *et al.* (1992). The static results from Alvappillai *et al.* (1992) are referred to as “Ref.: Static”. Analogously, the dynamic results for moving mass and moving force are referred to as “Ref.: Moving mass” and “Ref.: Moving force”, respectively. The numerical results obtained by this work are referred to as “Implemented model”.

3.1 Effect of the modulus of subgrade reaction

The behavior of the rigid pavement for different values of the modulus of subgrade reaction (*k*) is presented in Figure 6. The pavement response was evaluated at point A.

E&S - Engineering and Science ISSN: 2358-5390 DOI: 10.18607/ES202099827 Volume 1, Edição 9

Figure 6 - Normalized vertical deflections as a function of the normalized modulus of subgrade reaction

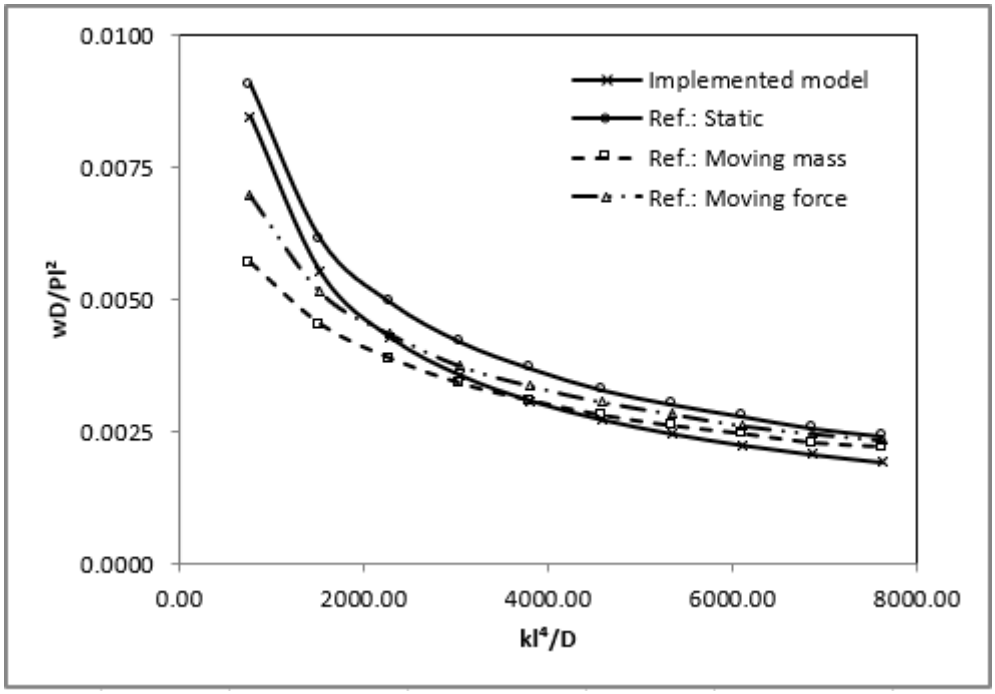

The global stiffness (*D*) of the pavement had to be estimated before plotting the results, since it is not provided by the work of Alvappillai *et al.* (1992). By reading each of the ten kl^4/D points obtained from Alvappillai *et al.* (1992) and knowing that *k* varies from 13572.352 kN/m³ to 135723.517 kN/m³ and *l* equals 7.620 m, *D* could be estimated by averaging the numerical readings, i.e. $D = D_{average}$ = 60007.461 kN*m.

From Figure 6, it can be noted that the increase in the modulus of spring reaction (k) representative of the subgrade medium induces, at first, a decrease in vertical deflections, but then stabilizes them. This behavior was quite expected because the increase in *k* makes the pavement-subgrade stiffer and, therefore, less susceptible to vertical deflections. This decrease, though, becomes negligible when the normalized subgrade modulus is higher than 8000 and the normalized pavement thickness is higher than 0.08.

The results from the model implemented in this work were expected to be similar to those of the static model, i.e. Ref.: Static (ALVAPPILLAI *et al.*, 1992). Nevertheless, nothing can be inferred as to which curve corresponds more closely to the curve of the implemented model in terms of physical behavior. At the beginning, the numerical results obtained herein are in excellent agreement with the static model. However, as *k* increases, this agreement becomes more evident with the moving force and moving mass results, that is, Ref.: Moving force and Ref.: Moving mass. It can be asserted, thus, that the increase in *k* does not generate significant dynamic effects.

In addition, the plate-type finite element used by Alvappillai *et al.* (1992) has only three degrees of freedom (*z*, θ_x and θ_y), and the beam elements used to represent the doweled joints only two (*z* and θ_x). The fact that the finite elements considered in this work have more degrees of freedom and are higher in number may have led to the divergences in vertical deflections observed in Figure 6, despite the finite element mesh being the same.

Figure 6 further shows that the lower the *k* values of the subgrade, the higher the normalized vertical displacements undertaken by the concrete plate, which highlights the relevance of using such plate (e.g. its material and geometry) as well as the doweled bars (e.g. material, geometry, number of bars) for the absorption of internal strains derived from the

E&S - Engineering and Science ISSN: 2358-5390 DOI: 10.18607/ES202099827 Volume 1, Edição 9

load applied. In other words, for a low *k*, the effect of the coupling elements between the plate and the subgrade becomes more evident.

3.2 Effect of the pavement thickness

Figure 7 illustrates the effect of varying the rigid pavement thickness on the vertical deflections (in the *z* direction) recorded at point A. This verification was performed analyzing thicknesses of 0.152 m and 0.610 m, and the results were obtained using the reference models (ALVAPPILLAI *et al.*, 1992) and the one implemented herein.

Figure 7 - Normalized vertical deflections as a function of the normalized pavement thickness

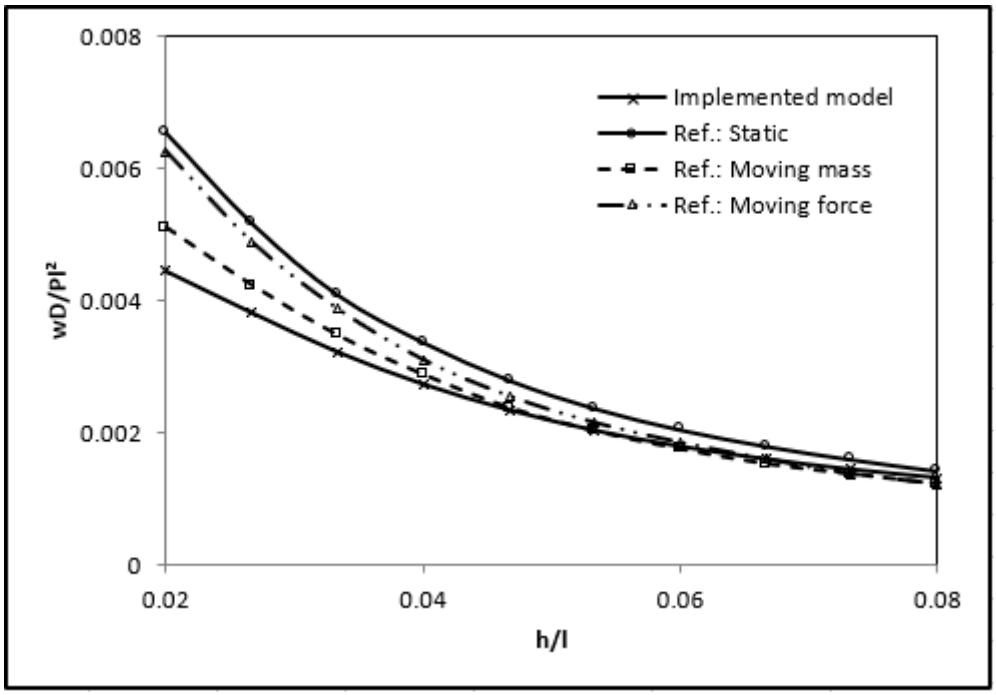

As it can be inferred from Figure 7, the higher the parametrized pavement thickness (*h*), the lower the parametrized vertical displacement (*w*); which was expected since the place becomes stiffer as the pavement thickness increases. In addition, as *h* increases, the parametrized deflections of the rigid pavement tend to stabilize following a smoother curve.

Once again, the physical behavior of the parametrized deflections from the implemented model were expected to be in agreement with the reference model Ref.: Static. Nevertheless, Figure 7 shows a good agreement with the reference moving mass model, i.e. Ref.: Moving mass. The existing divergences between the implemented model and the Ref.: Static model become less evident as *h* increases, and may be explained through the same arguments used in Section 3.2.

The discrepancy between the normalized vertical displacements of the implemented model and those from the reference model decreases as the parametrized pavement thickness increase. For higher *h* values, the stiffness of the material also increases since the support layer now has less influence compared with the concrete slab. In other words, as *h* increases, so does its structural stiffness, which will make this element absorb the internal strains more efficiently.

3.3 Effect of the transverse joints

Figure 8 shows the vertical deflections (*w*) along the longitudinal axis of the concrete slab (direction *x*, as illustrated in Figure 2) using the implemented and reference models,

obtained by modifying the position of the load application as well as the nodal point where the pavement deflections are recorded.

Figure 8 - Normalized vertical deflections along the normalized longitudinal axis of the rigid pavement

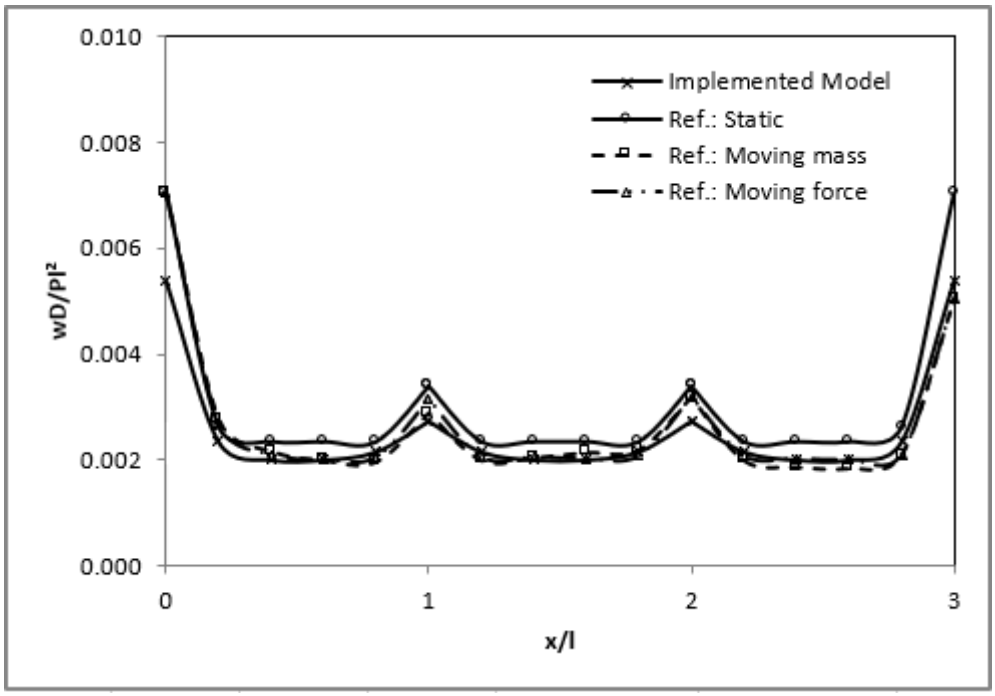

From Figure 8, the curve of normalized deflections obtained by the implemented model is very close to those of the reference models, especially the Ref.: Moving mass and Ref.: Moving force. It can also be noted from the figure that, similarly to the Ref.: Static curve, the curve obtained from the implemented model is symmetric, what is justified by the fact that model presents a symmetry with respect to its geometry and the position of the load application within the *x* direction. However, such symmetric behavior does not occur in the Ref.: Moving mass and Ref.: Moving force curves, which may indicate that the pavement response according to these models takes into account vertical deflections previously obtained, that is to say, it depends on the history of deflections generated by the moving aircraft load.

Figure 8 also depicts that the pavement deflections reach their maximum value at the lateral ends with no transverse joint. This might occur because at those points there are neither elements representative of the subgrade medium nor adjacent plate elements to absorb the displacements, what makes the deflections relatively higher. On the other hand, for the two superimposed elements at the transverse joint, the vertical deflections are lower, since the doweled bars transfer a portion of the applied load to the adjacent concrete slab. Finally, when the load is applied to the plate element, the vertical deflections are lower than the previous situations, because the plate has increased capacity for resisting them.

3.4 Effect of the diameter of doweled bars

Figure 9 shows the normalized vertical deflections along the transversal axis of the concrete slab (direction *y*, as illustrated in Figure 2) using the implemented model for different normalized diameters of doweled bars. The figure additionally compares the results obtained using the Ref.: Static model (curves named Ref.: d/h=0.042, Ref.: d/h=0.083, Ref.: d/h=0.125 and Ref.: Free edge) and those from the model implemented herein. The constants *a* and *m* are, respectively, the distance (*y*) from the edge of the plate to the point analyzed, and

E&S - Engineering and Science ISSN: 2358-5390 DOI: 10.18607/ES202099827 Volume 1, Edição 9

the plate width (7.620 m). The parameter *d* represents the varying diameter of the doweled bars and *h* the thickness of the rigid plate (0.305 m).

Figure 9 - Normalized vertical deflections along the pavement transverse joint considering different diameters of doweled bars

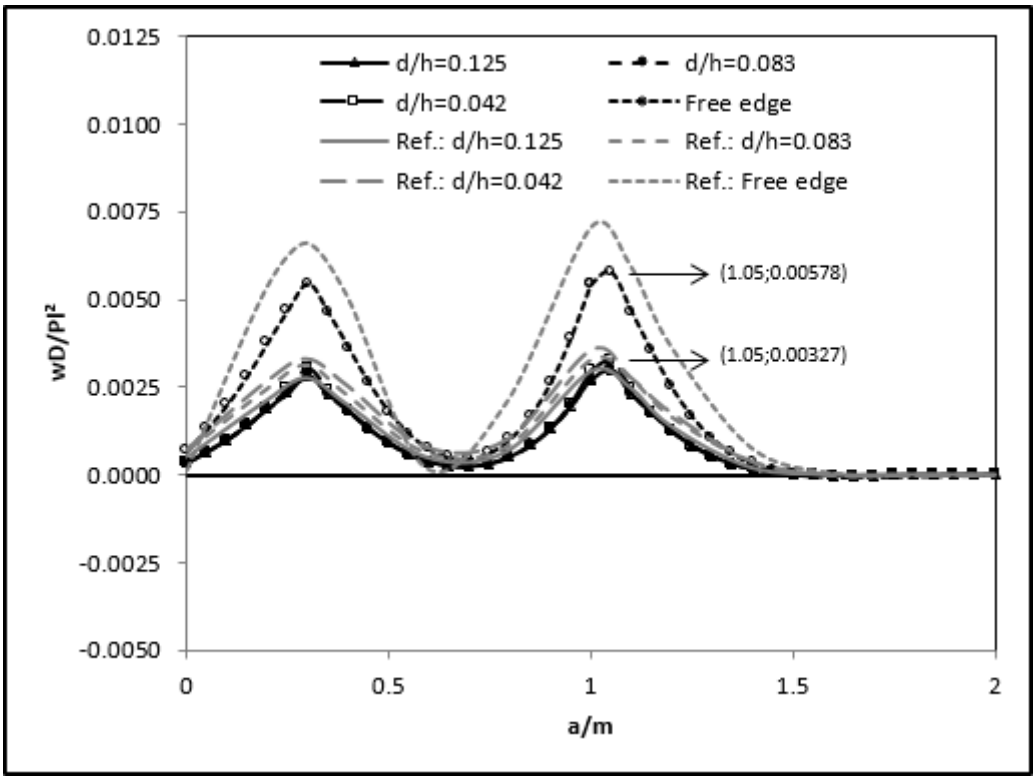

It can be seen from Figure 9 that the maximum normalized vertical deflections occur beneath the point where the aircraft moving load is applied. The point of maximum deflection obtained using the implemented model (0.00327) does not change significantly when *d*/*h* varies from 0.125 to 0.042, in other words, it is not influenced by the change in the diameter of doweled bars. The same behavior appears when reference models are employed. At the free edges, i.e. where there are no doweled bars, the vertical deflection jumps to 0.00578 for the implemented model, a 76.76% increase compared to the cases where *d*/*h* varies.

The discrepancies between the implemented and reference models from Alvappillai *et al.* (1992) are believed to be due to:

a) the length adopted for the doweled bars in the implemented model, i.e. 1.019 m, likely to be different from that of the reference models in which it is not provided;

b) the difference between the degrees of freedom and type of finite elements compared to the reference models. It should be noted that the elements used in this work and, thus, the degrees of freedom, are higher in number;

c) the fact that the number of spring-damper elements adopted for modeling the interaction between the subgrade medium and the concrete slabs are considerably higher in this work. In addition, no convergence analysis of the number of spring-damper elements is provided by Alvappillai *et al.* (1992), that is, the relatively smaller number of coupling elements in their work may have generated a less resistant soil and, therefore, higher vertical deflections at the edges and points where the moving aircraft load is applied (see Figures 8 and 9).

From the results depicted in Figure 8 and, particularly, Figure 9, the influence of the diameter of doweled bars on the normalized vertical displacements of the concrete slab is small compared with the influence of the modulus of subgrade reaction (specially for

situations where the normalized *k* values are higher than 2000, vide Figure 6) and of the pavement thickness (Figure 7). For situations involving relatively lower *k* values, the influence of the doweled bars on the normalized vertical displacements cannot be neglected.

3.5 Minimum characteristic strength of concrete according to Mohr-Coulomb's failure criterion

The Mohr-Coulomb failure criterion was employed to estimate the minimum compressive strength of the concrete pavement system required to withstand the dynamic load applied. Using this theory, established by simplifying the Mohr theory, a line is drawn tangent to the Mohr circles in failure condition obtained through tensile and compression laboratory tests, i.e. Mohr failure envelope. This envelope is therefore a mechanical characteristic of the employed material. According to the Mohr-Coulomb theory, failure of the material occurs if a Mohr circle is just tangent to the Mohr-Coulomb envelope.

This failure criterion states that brittle materials (such as concrete) will fail if the following general expression is satisfied (BEER *et al.*, 2015): $(\sigma_1/S_{ut} - \sigma_3/S_{uc}) > 1/n$, where σ_1 and σ_3 are the maximum and minimal principal stresses, respectively, S_{ut} is the module of the tensile ultimate strength, S_{uc} is the module of the compressive ultimate strength, both obtained experimentally, and *n* is the factor of safety (taken as 1 in the present work).

The Mohr-Coulomb failure criterion embodies the concepts of normal principal stresses and is applied to brittle materials for which S_{ut} and S_{uc} are different, as well as to structures in which the specific deformation (ε) is lower than 0.05. It is considered more conservative than the Modified Mohr theory (also known as Modified Mohr-Coulomb theory), in which failure is assessed through torsion tests.

For ductile materials, S_{ut} and S_{uc} are replaced by S_{YT} (tensile yield strength) and S_{YC} (compressive yield strength), respectively. The general equation for the Mohr-Coulomb failure criterion is the same as the Maximum Tangential Stress criterion.

The representation of the Mohr-Coulomb criterion on the principal stress axes can be reduced to (Budynas and Nisbett, 2015): **(1)** $\sigma_1 \geq \sigma_2 \geq (\sigma_3 = 0)$, and, if $\sigma_3 = 0$, the expression becomes $\sigma_1 > n.S_{ut}$; **(2)** $\sigma_1 \geq (\sigma_2 = 0) \geq \sigma_3$, which is the case represented by the general expression, and **(3)** $(\sigma_1 = 0) \geq \sigma_2 \geq \sigma_3$, in which the general expression is now reduced to $\sigma_3 < -n.S_{uc}$. Further details regarding the Mohr-Coulomb and other failure criteria applied to brittle and ductile materials can be found in Beer *et al*. (2015) and Budynas and Nisbett (2015).

Figures 10 and 11 illustrate the distribution of principal stresses (σ_1 and σ_3) according to the implemented model. The aircraft dynamic load was positioned as close to point A as possible and results were obtained after 30 s, i.e. the time required to attain stabilization of deflections. In the simulations, the thickness of the concrete slab is 0.305 m, the modulus of spring reaction representative of the subgrade medium is 81434.112 kN/m³ and the diameter of doweled bars is 2.540×10^{-2} m.

E&S - Engineering and Science ISSN: 2358-5390 DOI: 10.18607/ES202099827 Volume 1, Edição 9

Figure 10 - Distribution of the maximum principal stress (σ_1) along the rigid pavement

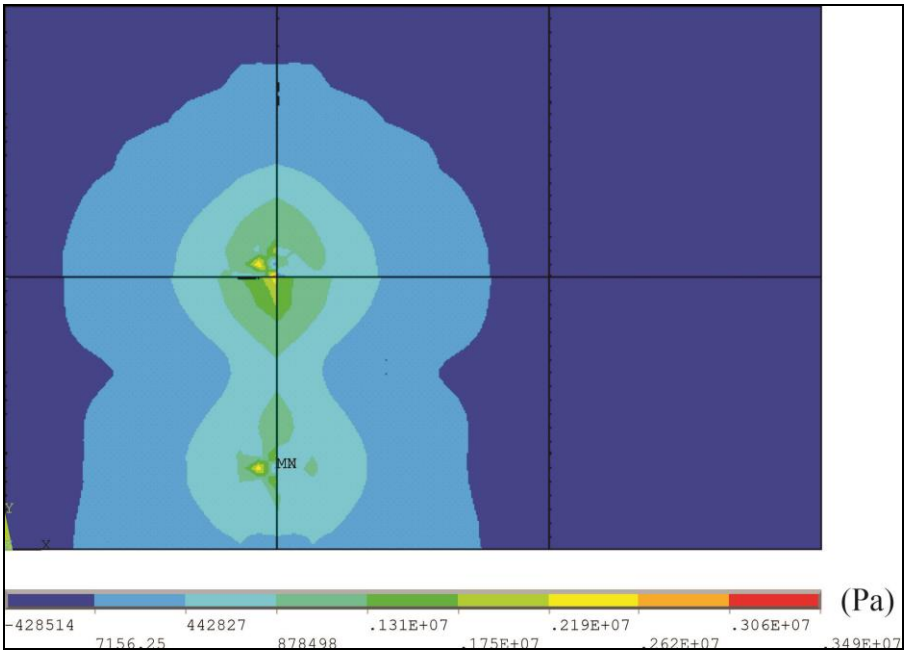

Figure 11 - Distribution of the minimum principal stress (σ_3) along the rigid pavement

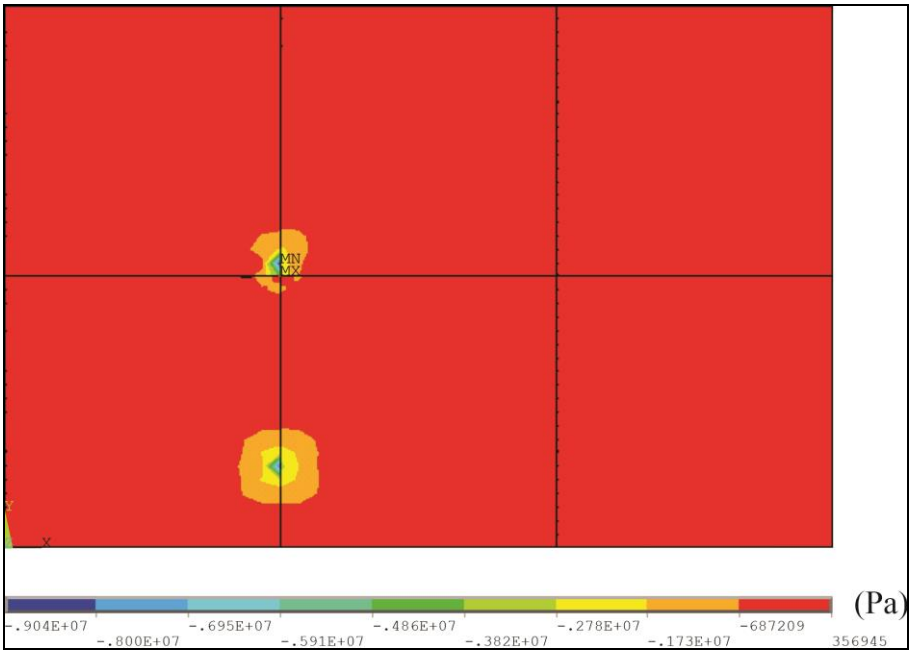

From Figures 10 and 11, the maximum principal stress (σ_1) occurring in the rigid slab reaches a peak value of 3.493 MPa, while the minimum principal stress (σ_3) of 9.040 MPa. Figure 10 suggests that tensile strains are developing at the points where the aircraft load is applied, aspect that must not be neglected during the design of the pavement system since concrete has significantly lower tensile strength.

The compressive strength of concrete (σ_{rc}) was assumed to be equivalent to the f_{ck} parameter from the expression $E = 5600\sqrt{f_{ck}}$ (MPa), where E is the Young's Modulus and f_{ck} the characteristic compressive strength of concrete specimens tested at 28 days (ABNT, 2014). Since E is 24,821.117 MPa, that results in a characteristic compressive strength (and, thus, σ_{rc}) of approximately 20 MPa, value often adopted for structural concrete design. The tensile strength of concrete (σ_{rt}) was assumed as 10% the f_{ck} value, i.e. 2 MPa. Hence,

according to the Mohr-Coulomb's failure criterion: (3.493/2 – 9.040/20) = 1.294 > 1, that is to say, the concrete pavement system would not resist the aircraft moving load for this set of strength parameters.

Figure 12 depicts the Mohr-Coulomb's failure coefficient, i.e. the left side of the Mohr- Coulomb's failure criterion, plotted against pavement thickness for different σ_{rc} values in order to determine the critical compressive strength of the concrete material simulated herein.

Figure 12 - Mohr-Coulomb's failure coefficient against pavement thickness for different σ_{rc} values (modulus of subgrade reaction equals 81434.112 kN/m³ and the aircraft considered is the B727 model)

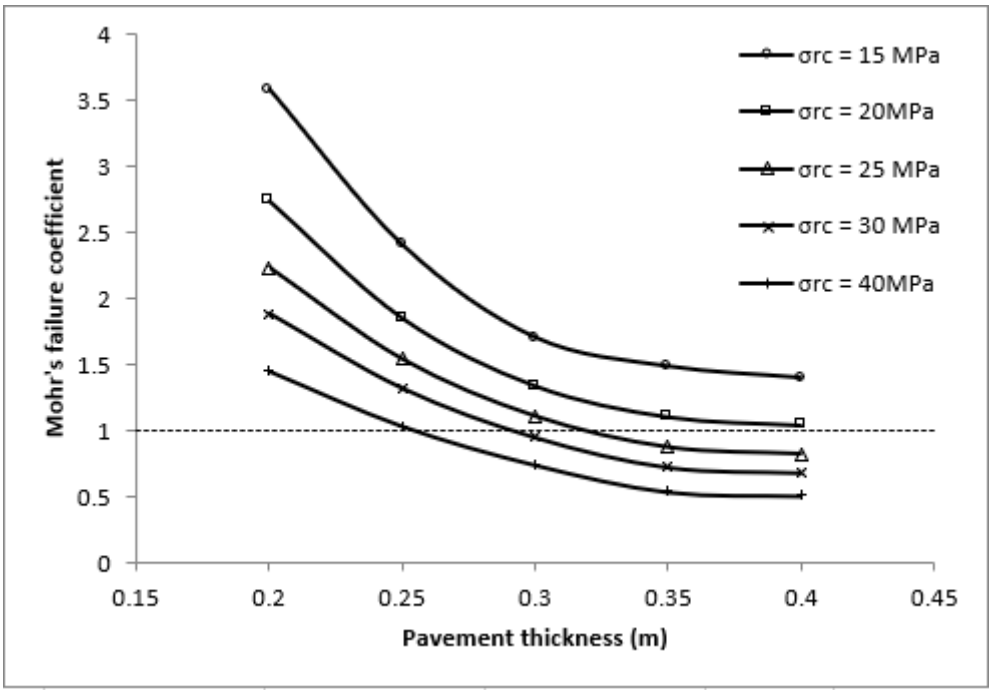

As it can be inferred from Figure 12, the higher the thickness of the rigid pavement the lower the Mohr-Coulomb's failure coefficient. Also, as the compressive strength (σ_{rc}) increases, the referred coefficient decreases for a given thickness, in other words, the higher the σ_{rc} value the smaller the critical thickness in the pavement design.

For the present model, the use of low σ_{rc} values (15 and 20 MPa) would imply adopting a pavement thickness considerably high in order to guarantee structural integrity (thicker than 0.400 m), which is impractical. From Figure 12, the σ_{rc} of concrete to be used in the design of pavement slabs with thickness (h) of 0.305 m is approximately 28 MPa. Such σ_{rc} would prevent concrete failure according to the Mohr-Coulomb's criterion.

The analysis of concrete failure presented in this section is merely a hypothetical assessment of whether or not the rigid pavement system considered in the simulations would resist the aircraft load. Furthermore, the results obtained are only valid for the load position adopted in the simulations and a thorough design would require the analysis of other points along the structure. It serves the one and only purpose of illustrating how to predict, from the state of plane stress illustrated in Figures 10 and 11, the effects on the simulated concrete slabs.

4. CONCLUSIONS

In the present work, the finite element method (FEM) was employed to model the dynamic response of aerodromes pavements subjected to a B727 load. The pavement system consisted of six concrete slabs connected by doweled bars at the transverse joints and by aggregate interlock or keyed joints at the longitudinal joints. Concrete slabs were idealized by solid plate elements resting on Kelvin-type viscoelastic elements representing the subgrade medium. The doweled bars and keyed or aggregate interlock joints are modeled by beam and vertical spring elements, respectively.

The influence of the diameter of doweled bars, longitudinal joints and stiffness of the subgrade medium in light of the results of vertical deflections was discussed and compared with the work of Alvappillai *et al*. (1992). Discrepancies were found and are believed to be mainly due to: (1) the fact that the elements used in this work and, thus, the degrees of freedom, are higher in number; (2) the lack of information from the reference model, particularly concerning the length of doweled bars, which might have provided additional stiffness to the concrete slabs (specially for low modulus of subgrade reaction, *k*) and (3) the distribution of *k*, which also might have added stiffness to the model.

The variation of parametrized diameters of doweled bars (from d/h=0.042 to d/h=0.125, considering the thickness h of concrete slabs of 0.305 m) did not affect the pavement vertical deflections significantly. However, the absence of doweled bars generated approximately 77% increase in such deflections. Longitudinally, maximum vertical deflections occurred at the lateral ends with no transverse joints, that is to say, at the zones where neither the subgrade medium nor adjacent plate elements are able to absorb the displacements.

Additionally, an increase in the modulus of subgrade reaction as well as in the thickness of concrete slabs led to a decrease in vertical deflections. Such decrease, though, became negligible when the normalized subgrade modulus was higher than 8000 and the normalized pavement thickness was higher than 0.08, approximately.

Finally, the normal stresses developed as a result of the aircraft load were computed using the Mohr-Coulomb's failure criterion based on the Elasticity Theory for small deformations and brittle materials. It was observed that the increase in both the minimum compressive strength of concrete (σ_{rc}) and pavement thickness induces a decrease in the Mohr-Coulomb's failure coefficient, i.e. the higher the σ_{rc} value the smaller the critical thickness in the pavement design. For the present set of pavement-subgrade properties, the σ_{rc} value for a design thickness of 0.305 m should be 28 MPa.

5. ACKNOWLEDGEMENTS

The authors gratefully thank the Federal University of Triângulo Mineiro (UFTM) for providing the physical space for the numerical simulations.

6. REFERENCES

ABNT - ASSOCIAÇÃO BRASILEIRA DE NORMAS TÉCNICAS. **NBR 6118.** Projeto de estruturas de concreto – Procedimento. RJ, *Associação Brasileira de Normas Técnicas*, 2014.

ALVAPPILLAI, A.; ZAMAN, M.; LAGUROS, J. Finite element algorithm for joited concrete pavements subjected to moving aircraft. **Computers and Geotechnics,** v.14, n. 3, p. 121-147, 1992. doi.org/10.1016/0266-352X(92)90030-W

ANSYS. **ANSYS Help: Mechanical APDL Documentation**. 2018.

BALBO, J. T. **Pavimentos de concreto.** 1st ed. São Paulo: Ed. Oficina de Textos, 2009.

BEER, F.; JOHNSTON Jr., E. R.; DEWOLF, J.; MAZUREK, D. **Mechanics of Materials.** 7th Ed., New York: McGraw-Hill Education, 2015**.**

BUDYNAS, R. G.; NISBETT, J. K. **Shigley's Mechanical Engineering Design**. 10th Ed., New York: McGraw-Hill Education, 2015.
CALIENDO, C.; PARISI, A. Stress-Prediction Model for Airport Pavements with Jointed Concrete Slabs. **Journal of Transportation Engineering**, v. 136, n. 7, p. 664-677, 2010. doi: 10.1061/(ASCE)TE.1943-5436.0000151

DELATTE, N. **Concrete Pavement Design, Construction and Performance**. 1st ed. New York: Ed. Taylor&Francis, 2008.

KANDEKAR, S. B.; TALIKOTI, R. S. Torsional behaviour of reinforced concrete beam wrapped with aramidfiber. **Journal of King Saud University:Engineering Sciences**, v. 3, n. 4, p. 340-344, 2019. doi: 10.1016/j.jksues.2018.02.001

KIM S. H.; PARK J. Y.; JEONG J. H. Effect of temperature-induced load on airport concrete pavement behavior. **KSCE Journal of Civil Engineering**, v.18, n.1, p.182-187, 2014. doi: 10.1007/s12205-014-0056-7

KIM, J.; HJELMSTAD, K. D. Three- Dimensional Finite Element Analysis of Doweled Joints for Airport Pavements. **Annual Meeting of Transportation Research Board.** Washington, D.C. Publication in Transportation Research Record, 2003. doi: 10.3141/1853-12

MAHMOUD, A. M. Finite element implementation of punching shear behaviors in shear-reinforced flat slabs. **Ain Shams Engineering Journal**, v. 6, p. 735-754, 2015. doi: 10.1016/j.asej.2014.12.015

PRAWESTI, P.; SUHENDRO, B.; HAPSORO, S. Evaluation of rigid pavement on apron of terminal 3 Soekarno-Hatta International Airport using finite element method. **MATEC Web of Conferences**, v. 270, 2019. doi: 10.1051/matecconf/201927003005

RODCHENKO, O. Computer Technologies for Concrete Airfield Pavement Design. **Journal Aviation**, v. 21, n. 3, p. 111-117, 2017. doi: 10.3846/16487788.2017.1379439

SILVA, S. C.; BANDEIRA, A. A. Analyses of reinforced concrete beams strengthened with CFRP under bending: theorical and computational approaches. **Revista Ibracon de Estruturas & Materiais,** v. 12, n. 2, p. 233-254, 2019. doi: 10.1590/s1983-41952019000200003

YAN-CONG, Z.; LING-LING, G. Effect of dowel bar position deviation on joint load-transfer ability of cement concrete pavement**. International Journal of Pavement Research and Technology**, v. 9, n. 1, p. 30-36, 2016. doi: 10.1016/j.ijprt.2016.01.002